Project 5 - FYS4150
Numerical solution of the two-dimensional Schrödinger equation

Nanna Bryne, Johan Mylius Kroken, Vetle A. Vikenes
(Dated: December 14, 2022)

Simulations of the temporal evolution of wave functions that satisfy the two-dimensional Schrödinger equation on a discretised spatial grid, obeying Dirichlet boundary conditions. This partial differential equation (PDE) is solved numerically using the Crank-Nicolson method, which proves reliable as the deviation in the expected total probability over time is close to machine precision. An initialised wave packet is propagated through a zero-potential, showing dispersive behaviour, as well as through single-, double- and triple-slit configurations, for which the observed diffraction patterns resemble well known wave behaviour.
Supporting material may be found in the following GitHub repository: https://github.com/Vikenes/FYS4150/tree/main/project5.

I. INTRODUCTION

As with all good stories, this too starts in Ancient Greece, where Democritus laughingly[1] postulated the world to be made up of tiny, indestructible elements; atoms [1]. Along with this followed a description of the universe where everything was made up of these atoms. With the discovery of smaller and smaller building blocks came the desire to truly understand the workings of nature on a microlevel. This was formalised with the theory of quantum mechanics in the first half of the 20^{th} century [5], challenging established concept of physics like causality and deterministic behavioural descriptions of particles.

This was manifested through the otherwise well-known double-slit experiment, where you propagate particles through two thin slits, and record whatever pattern they make onto a screen on the other side of the slits. For particles of substantial size, each slit gave rise to a band on the screen, as we would intuitively expect. However, for smaller particles (first discovered with electrons), the pattern recorded turned out to be a diffraction pattern, similar to the patterns created by liquids (and light), indicating wave-like behaviour of the electrons.

This wave-like behaviour is encompassed into the so-called *wave function*, whose spatial and temporal dynamics are described with the Schrödinger equation. The aim of this report is to solve this equation in a confined spatial environment, effectively evolving the wave function in time. We will propagate a Gaussian wave packet through different slit configurations in order to replicate the interference pattern caused by the dispersive and diffractive behaviour of the particles, similar to those exhibited by liquids and light.

The outline of this report will be as follows: We provide a brief theoretical motivation in section II. Section III will be all about the methods we use, and how we discretise and solve the Schrödinger equation on a two-dimensional grid. It is divided into two subsections, section III A which is about discretisation (section III A 1) and implementation (section III A 2) of the numerical scheme. Section III B is about the initialisation of the system (section III B 1), the slit configuration (section III B 2), the detector screen (section III B 3) and the simulation itself (section III B 4). We present the results and sanity checks in section IV. In section V we provide a brief discussion, and finally, a conclusion in section VI. There are also two appendices explaining the Crank-Nicolson discretisation (appendix A) and the explanation of the matrices A and B (appendix B) used to solve our system.

II. THEORY

For a single, non-relativistic particle with mass m_{P} in a two-dimensional potential $\mathcal{V}(t, \mathbf{x})$, the Schrödinger equation reads:[2]

$$\mathrm{i}\hbar\frac{\partial}{\partial t}\Psi(t,\mathbf{x}) = -\frac{\hbar^2}{2m_{\text{P}}}\nabla^2\Psi(t,\mathbf{x}) + \mathcal{V}(t,\mathbf{x})\Psi(t,\mathbf{x}). \quad (1)$$

For a set of initial and boundary conditions, the partial differential equation (PDE) describes the temporal and spatial evolution of the complex-valued (wave) function $\Psi(t, \mathbf{x})$ related to the quantum state of the aforementioned particle. In such a case, at a time t, the probability density for an experimentalist to locate the particle at $\mathbf{x}$ is

$$P(\mathbf{x};\, t) = |\Psi(t,\mathbf{x})|^2 = \Psi^*(t,\mathbf{x})\Psi(t,\mathbf{x}), \quad (2)$$

originating from the Born rule.

In this report we will consider a dimensionless time-independent potential, i.e. we let $\mathcal{V}(t, \mathbf{x}) \to v(\mathbf{x})$. The specifics of the scaling do not concern us here, and we simply rewrite equation (1) to the dimensionless equation

$$\mathrm{i}\frac{\partial}{\partial t}u(t,\mathbf{x}) = -\nabla^2 u(t,\mathbf{x}) + v(\mathbf{x})u(t,\mathbf{x}), \quad (3)$$

[1] This is hypothetical, but plausible as he was known as the "laughing philosopher".

[2] In position space, that is.

where we substituted $\Psi(t, \mathbf{x}) \to u(t, \mathbf{x})$. In equation (3) all variables are dimensionless. When demanding the proper normalisation on $u(t, \mathbf{x})$, it follows that the Born rule now takes the form of

$$p(\mathbf{x};\, t) = |u(t, \mathbf{x})|^2 = u^*(t, \mathbf{x})u(t, \mathbf{x}). \tag{4}$$

In this report we will refer to $u(t, \mathbf{x})$ as the *wave function*, which is the solution of the dimensionless Schrödinger equation from equation (3). The aim is to solve for $u(t, \mathbf{x})$ in a confined space, with and without slits, and simulate the time evolution of Gaussian wave packets in this space. We will focus on solving this equation as a regular two-dimensional partial differential equation, and not delve much into details of quantum mechanics. As for the probabilities we will use both the terms probability, probability distribution and probability density to describe the quantity represented by equation (4).[3]

III. METHODS

We will solve the dimensionless wave function from equation (3) on a two-dimensional grid. Through the Born rule, equation (4), we may from the wave function construct the probability of finding a particle somewhere on this grid. We confine the particle by imposing Dirichlet boundary conditions (to be defined). In order to investigate the behaviour of the wave function we place two or more walls inside the box to create one or more slits. The specifics of such configurations is elaborated in section III B 2. A point inside the box is called $\mathbf{x} = (x, y)$ and the time is t, all unitless quantities. Now $x, y \in [0,\, L]$ and $t \in [0,\, T]$. For simplicity we will use $L = 1$, and T is the time we simulate for.

A. Numerical scheme

1. Discretisation

We discretise the position $\mathbf{x} \to \mathbf{x}_{i,j} = (x_i, y_j) = h(i, j)$, where h is the spatial separation between two points on the grid and i and j are integers. We consider M points in each direction, giving $i, j \in [0,\, M)$, resulting in $M-1$ steps and $M-2$ internal points. The lattice is then made up of $(M-2) \times (M-2)$ internal points in addition to boundary points. The time points become $t \to t_n = n\Delta t$, where Δt is the time step size and $N_t = T/\Delta t$ is the number of time points, so that the integer time steps are $n \in [0, N_t)$. In discretised form, we now write the wave function, probability density and potential as

$$u(t, \mathbf{x}) \to u(t_n, \mathbf{x}_{i,j}) \equiv u_{i,j}^{(n)}, \tag{5}$$

$$p(\mathbf{x};\, t) \to p(\mathbf{x}_{i,j};\, t_n) \equiv p_{i,j}^{(n)}, \tag{6}$$

$$v(\mathbf{x}) \to v(\mathbf{x}_{i,j}) \equiv v_{i,j}, \tag{7}$$

where the superscript (n) refers to the time index. We will consider discretised quantities for the remainder of this report. We will therefore denote quantities both with and without subscripts, depending on whether we want to emphasize specific indices or not.

2. Implementation

In order to solve equation (3) numerically on a discretised grid, as explained above, we use the Crank-Nicolson method. A detailed derivation of the method we implement is given in appendix A. It allows us to express the time evolution of the system as:

$$u_{i,j}^{(n+1)} - \mathcal{F}_{i,j}^{(n+1)} = u_{i,j}^{(n)} + \mathcal{F}_{i,j}^{(n)}, \tag{8}$$

where

$$\begin{aligned} \mathcal{F}_{i,j}^{(n)} = \quad & r\left(u_{i+1,j} - 2u_{i,j} + u_{i-1,j}\right)^{(n)} \\ & + r\left(u_{i,j+1} - 2u_{i,j} + u_{i,j-1}\right)^{(n)} \\ & - \frac{\mathrm{i}\Delta t}{2} v_{i,j}\, u_{i,j}^{(n)}, \end{aligned} \tag{9}$$

and we have defined $r \equiv \frac{\mathrm{i}\Delta t}{2h^2}$. This time evolution is valid for any time step with the time range $n \in [0, N_t - 2]$. Its spatial validity is restricted to the internal points of the grid; $i, j \in [1, M-2]$. For the boundary points we impose the Dirichlet boundary conditions which are:

$$u(t, \mathbf{x}_{0,j}) = u(t, x{=}0, y) = 0,$$

$$u(t, \mathbf{x}_{M-1,j}) = u(t, x{=}1, y) = 0,$$

$$u(t, \mathbf{x}_{i,0}) = u(t, x, y{=}0) = 0 \text{ and}$$

$$u(t, \mathbf{x}_{i,M-1}) = u(t, x, y{=}1) = 0.$$

If we then define

$$\begin{aligned} \mathbf{u}^{(n)} \equiv [&u_{1,1}^{(n)}, \ldots, u_{M-2,1}^{(n)}, \ldots, \\ &u_{1,M-2}^{(n)}, \ldots u_{M-2,M-2}^{(n)}], \end{aligned} \tag{10}$$

to be the column vector with dimension $((M-2)^2 \times 1)$ that contains all $u_{i,j}^{(n)}$ values for the internal points on the grid.[4] This, combined with the boundary conditions

[3] "Probability density" will technically be wrong since we solve for a two-dimensional lattice where each lattice point represent a spatial area of h^2, and the probability measured is the probability that the particle is confined within this are. However, we will use the terms interchangeably, and you are now warned.

[4] $u_k^{(n)}$ is the k^{th} element of $\mathbf{u}^{(n)}$ where $k = (j-1)\cdot(M-2)+(i-1)$ is valid for the internal points so that any $u_{i,j}^{(n)}$ has a corresponding $u_k^{(n)}$ for $i, j \in [1, N-1]$.

allows us to rewrite equation (8) into a matrix equation of the form:

$$A\mathbf{u}^{(n+1)} = B\mathbf{u}^{(n)}. \tag{11}$$

A and B are matrices, whose specific forms are governed by the particular problem we consider in this report. We refer to appendix B for a detailed description of these two matrices. We are now able to evolve the system in time by solving equation (11) in a time loop, which we divide into two steps:

$$\begin{aligned} &1.\ \text{Perform matrix multiplication: } \mathbf{b} = B\mathbf{u}^{(n)}. \\ &2.\ \text{Solve the matrix equation: } A\mathbf{u}^{(n+1)} = \mathbf{b}, \end{aligned} \tag{12}$$

where $\mathbf{u}^{(n+1)}$ is the unknown we solve for. When solving equation (12) we can use the structure of A to our advantage. A arise from a boundary value problem. We could use direct methods, such as Gaussian elimination or LU-decomposition. The latter may be used to compute the inverse, A^{-1}. This could be beneficial, since the constant A^{-1} would apply at all time steps. We could also use iterative methods such as the Jacobi method or Gauss-Seidel. A is diagonally dominant,[5] and we are thus guaranteed convergence with the Jacobi method [3]. However, noticing that the vast majority of the entries in A are zeros, we represent it numerically as a *sparse matrix*, only saving the indices and values of non-zero entries. This allows us to use the `spsolve()` method from the `Armadillo` library to solve equation (12). The method solves the system of sparse linear equations by a special algorithm for performing LU decomposition, called a Supernoidal LU decomposition (SuperLU) [4]. We refer to their article for a more detailed description of the algorithm.

B. Initialisation and simulation

Having addressed methods for advancing the system in time, we now turn our attention to how we initialise the system. Additionally, we describe how we model the slits in our simulation box.

1. Initial wave packet

The initialisation is done by imposing the following initial condition:[6]

$$\begin{aligned} u(t{=}0, \mathbf{x}) = \exp\{ &-(\mathbf{x}-\mathbf{x}_\mathrm{c})^\mathrm{T}\Sigma^{-1}(\mathbf{x}-\mathbf{x}_\mathrm{c}) \\ &+ \mathrm{i}\mathbf{p}^\mathrm{T}(\mathbf{x}-\mathbf{x}_\mathrm{c})\} \end{aligned} \tag{13}$$

where Σ, $\mathbf{x}_c$ and $\mathbf{p}$ are the spatial variance, spatial centre location and momentum of the initial wave packet, respectively, where we have defined $\Sigma \equiv \mathrm{diag}(\boldsymbol{\sigma}^2)$. This is a two-dimensional complex Gaussian wave packet. The parameters for different initialisations can be found in tables I and II. We normalise this initial state so that:

$$\sum_{i,j} u_{i,j}^{(0)*} u_{i,j}^{(0)} = 1, \tag{14}$$

which enables us to interpret $p_{i,j}^n = u_{i,j}^{(n)*} u_{i,j}^{(n)}$ as the probability that the particle is located in a small grid cell of size h^2, centred at (x_i, y_i), which is in accordance with the Born rule from equation (4).

2. Slit configuration

To create a *single* slit, we need *two* objects with the property that the wave packet cannot propagate through it. Said objects are to have a separation between them, a *slit*, perpendicular to the dominating motion of the wave packet. A natural choice for the shape of these objects are rectangles. The separation of these rectangles, or "walls", then give rise to the slits. Three such walls give rise to two slits, and so on. However, to achieve proper n-slit experiments, we should make sure that the two outermost walls of this setup reach the edges of the grid, so that the only way of bypassing the wall is through the slits.

A natural choice for modelling such walls is to set the potential at their grid positions to a high constant value. The slits can then be represented as zero-potential gateways through the large potential. We also set the potential to zero everywhere else in the box, meaning that the walls are the only place inside the box with a non-zero potential. We will make sure that the slit setup is symmetric around the box centre in both directions. Thus, say we want n slits, we would need $n-1$ identical wall pieces and two identical walls that closes the gap between the outer slits and the box edges.

3. Artificial detector screen

To reduce the dimensionality of the problem, we can assume to measure a particle with a detector screen at some horizontal position $x = x_\mathrm{sc}$ and time $t = t_\mathrm{sc}$, so that the screen spans of the vertical axis y. With a smart choice of pairing (t_sc & x_sc), we can safely assume that the particle is located somewhere along this line. Thus, it makes sense to consider a normalised one-dimensional probability function $p_{x=x_\mathrm{sc}}(y;\, t_\mathrm{sc})$ (read: probability of y given $x = x_\mathrm{sc}$, at $t = t_\mathrm{sc}$) such that

$$p^\mathrm{tot}_{x=x_\mathrm{sc}}(t{=}t_\mathrm{sc}) = \sum_{j\in[0,M)} p_{x=x_\mathrm{sc}}(y_j;\, t_\mathrm{sc}) = 1. \tag{15}$$

To study the expected diffraction pattern, it will be appropriate to choose a time and place right after the particle has passed through the slit(s). In the case with two

[5] See appendix B

[6] We stress that the initialisation also has to obey the boundary conditions.

slits, the setup imitates the famous double-slit experiment.

4. *Simulations*

We aim to run a few experiments and their common setup is presented in table I, where an asterisk is used to indicate that a certain parameter is related to a specific setup.

Simulation parameters	
Spatial step size (h)	$5.0 \cdot 10^{-3}$
Temporal step size (Δt)	$2.5 \cdot 10^{-5}$
Total time (T)	$*$
Slit configuration (following section III B 2)	
Number of slits (N_{slits})	$*$
Number of walls; inner + outer	$(N_{\text{slits}} - 1) + 2$
Wall dimensions; width×height	0.02×0.05[a]
Wall centre position	$(0.5, \sim 0.5)$[b]
Slit aperture; separation between walls	0.05
Potential inside barrier (v_0)	$1.0 \cdot 10^{10}$
Initial wave packet (the Gaussian in equation (13))	
Centre position ($\mathbf{x}_c$)	(0.25, 0.50)
Spatial extent ($\boldsymbol{\sigma}$)	$(0.05, *)$
Momentum ($\mathbf{p}$)	(200, 0)
Vertical screen (following section III B 3)	
Horizontal position (x_{sc})	0.8
Time point (t_{sc})	0.002

[a] The height of the outer walls will be different.
[b] Slit setup symmetric around $y = 0.5$.

TABLE I: Numerical values for static simulation parameters. Simulation-specific values are denoted "$*$".

The simulation specific parameters are presented in table II, where we also define the names that we will use to refer to each simulation.

Simulation name	(label[a])	N_{slits}	T	$\boldsymbol{\sigma} \cdot \hat{\mathbf{e}}_y$
1. No slits	(*NS*)	0	0.008	0.05
2. Double-slit (1)	(*DS1*)	2	0.008	0.10
3. Double-slit (2)	(*DS2*)	2	0.002	0.20
4. Single-slit	(*SS*)	1	0.004	0.20
5. Triple-slit	(*TS*)	3	0.004	0.20

[a] Prefix to look for amongst the animations.

TABLE II: Supplement to table I. Additional information about the simulations considered in this paper.

C. Initial validation

The total probability should be conserved in time, but small deviations are expected to occur from our numerical implementation. How well the probability is conserved will depend on the method chosen for solving equation (12), among other things. To assert that our implementations are reasonable, we will plot the deviations of $p(\mathbf{x}_{i,j};\, t)$ from the true analytical value of 1 as a function of time, namely

$$\left|1 - p^{\text{tot}}(t)\right|; \quad p^{\text{tot}}(t) = \sum_{i,j \in [0,M)} p(\mathbf{x}_{i,j};\, t). \tag{16}$$

We have omitted subscripts for the total two-dimensional probability to avoid confusion with the one dimensional probability introduced in equation (15). Our implementation of the potential barriers are may give rise to additional numerical inaccuracies. We therefore check our implementation by studying the total probability deviations when we have no barriers in the box, and when we have a double-slit in the box, i.e. three barriers. The double-slit we will consider for this analysis is (*DS1*).

IV. RESULTS

For the interested reader with a keen interest in visualisation, we present animations of the probability density resulting from each simulation listed in table II in our GitHub repository.[7] The different results presented in the following subsections are related to parameters that are given in table I and II.

A. Probability conservation

The first simulation, where there are no slits, gives deviations in $p^{\text{tot}}(t)$ with an order of $\sim 10^{-14}$, as seen in figure 1. In the case of the double-slit (*DS1*), we see from the figure that we get deviations that are somewhat smaller in magnitude. Both simulations yield deviations that are close to machine precision. These results imply that our numerical implementations are reasonable in a physical sense, and that the strength of the potential barriers is appropriate for the total probability to be conserved.

B. Two-dimensional problem

We now simulate the box with a double-slit (*DS2*), and present snapshots of the probability distribution $p(\mathbf{x};\, t)$

[7] https://github.com/Vikenes/FYS4150/tree/main/project5/output/videos

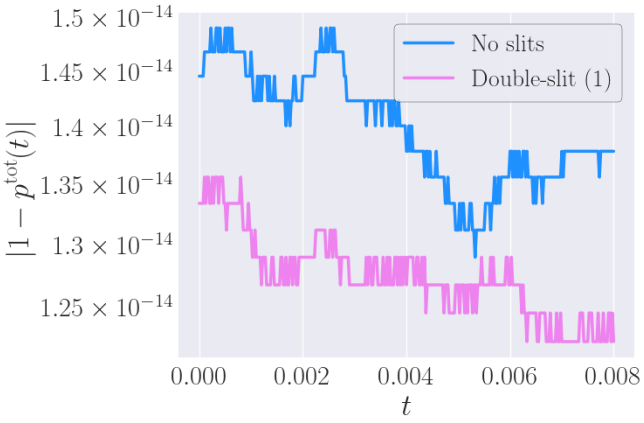

FIG. 1: *NS* & *DS1*: The total probability's deviation from the theoretical value, following equation (16), as function of time, for the two initial experiments. The vertical axis is logarithmic.

at $t \in \{0, T/2, T\}$, shown in figure 2a, with $T = 0.002$. In addition, the real and imaginary part of $u(t, \mathbf{x})$ at the same times are presented in figures 2b and 2c, respectively. Notice the large back-scattering in each plot, especially visible in the probability distribution plot (figure 2a).

We stress that the scales on the colour bars in figure 2 change between simulations. In figure 2a, the dark areas correspond to a low likelihood of detecting the particle, whereas the areas coloured yellow represent the places where one is most likely to find the particle. In the wave function components in figures 2b and 2c, negative values are coloured green, values close to zero are coloured navy and positive values have a light blue shade, roughly speaking. Note also that for all three quantities, the snapshot at $t = 0.001$ have a different scaling on the colour bar compared to the snapshots at the other two instances in time. The variations of the scales of the colour bars are chosen to better resolve the spatial distribution in the individual snapshots.

C. One-dimensional problem

Using the same parameters, we run two additional simulations, (*SS*) and (*TS*), except that we vary the number of slits (see tables I and II). In the following, we study the system further by removing one dimension. Take note of the dotted vertical line in the right panel of figure 2a. Following the method described in section III B 3, we find the probability distribution along this screen, which we plot as a function of y in figure 3b. The same screen is used for the single- and triple-slit experiments, resulting in the graphs in figures 3a and 3c respectively.

V. DISCUSSION

The sanity check represented by the graphs in figure 1 indicates that our solution is stable for $t \leq 0.008$. However, this result was only obtained from two particular simulation configurations. One of the main features in all our simulations were that we considered vertically symmetric wave packets propagating towards higher values of x. A more proper verification of our implementations would require tests with different initializations. Some natural choices for further investigation would be to consider wave packets initialized with a non-zero momentum in the vertical direction, as well as different choices for their vertical centre. Nonetheless, the initial testing provided desirable results within the scope of our analysis.

The animations show very different behaviours for *NS* and *DS1*. From the former to the latter, we can clearly see the effect of introducing slits and how the probability distribution navigates around the barriers. With no slits, we can clearly see the dispersive behaviour of the probability density in the y-direction. This effect is less noticeable when slits are present, as it's difficult to distinguish this feature from effects caused by interactions with the slits. It is worth noting that the large back-scattering present in the double slit simulations (and quite probably for the other slit configurations as well), occurs due to the initial wave packet being larger than the slit aperture for all the wave packets considered here.

When it comes to our choice of using the SuperLU method to solve the linear equations, this was an efficient way to deal with a complex aspect of the numerical implementations. One drawback with this choice is that we are left with little insight to the workings of our algorithm as a whole. For instance, figure 1 shows that the total probability deviates less when we had double slits, compared to the case when we had no slits. This seems to be a bit counterintuitive, and there may be several reasonable explanations for why we get this result. For one thing, our measurements of the deviations is not very informative, in the sense that we only measure the sum of absolute deviations. However, even with further improvements of the analysis, the SuperLU method prevents us from drawing assertive conclusions. This method utilizes concepts like partial pivoting, where the accuracy may depend on specifics of the configurations. Concluding about varying performance for different simulation configurations would thus require more extensive studies, where other numerical methods are considered.

VI. CONCLUSION

Through the Crank-Nicolson scheme, we have succeeded in building an algorithm that solves the time evolution of the quantum state initialised by a Gaussian wave packet existing in a two-dimensional box with a zero- to three-slitted (potentially more) barrier. The deviation in the total probability is insignificant for the

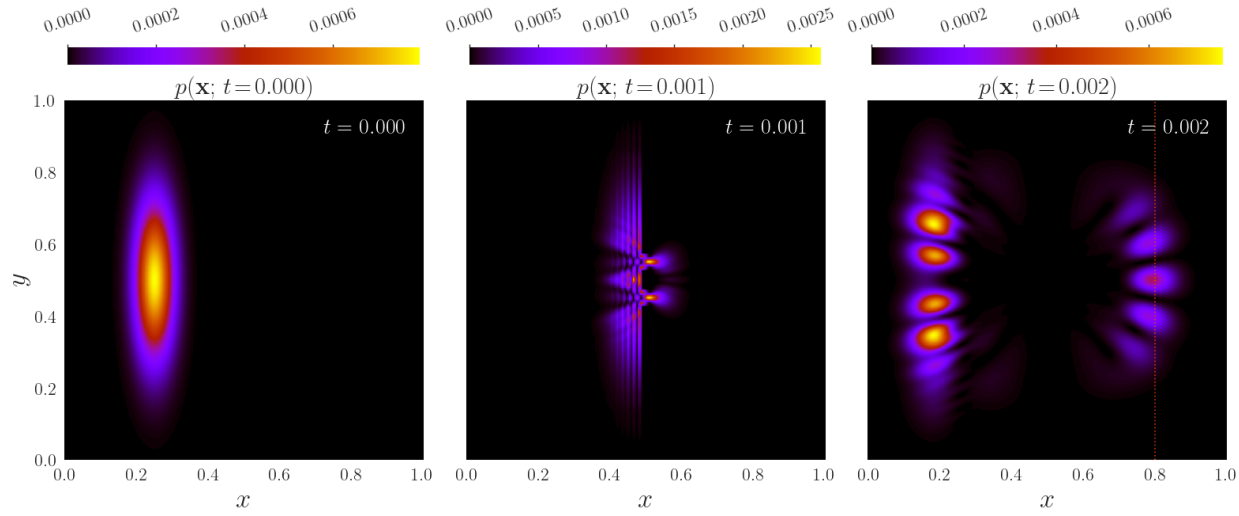

(a) *DS2*: Snapshots representing the evolution of the probability density. The dotted vertical line represents the screen we consider in figure 3.

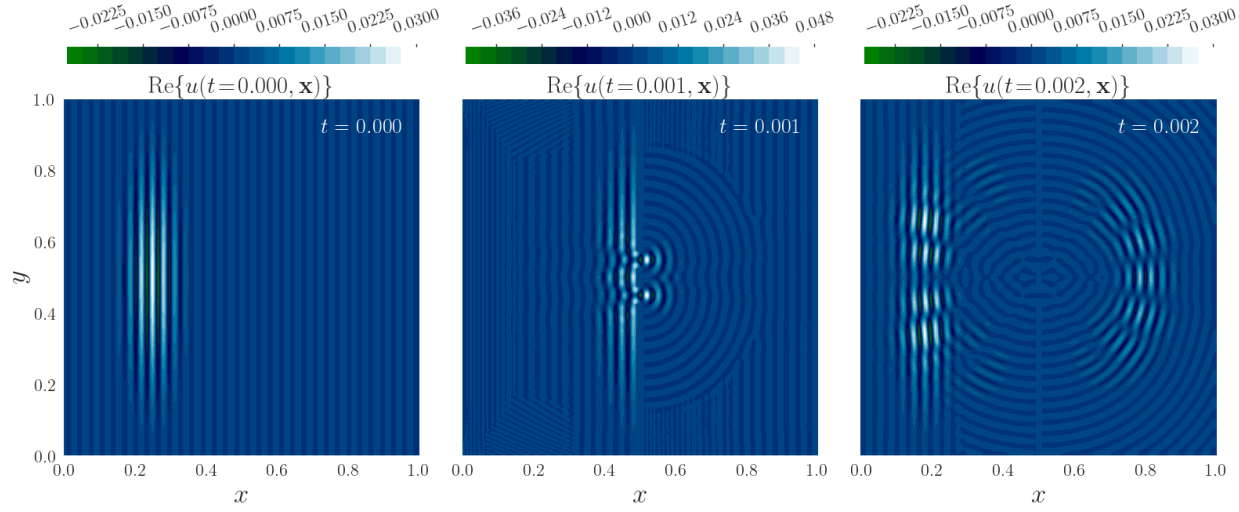

(b) *DS2*: Snapshots representing the evolution of the real part of the wave function in position space.

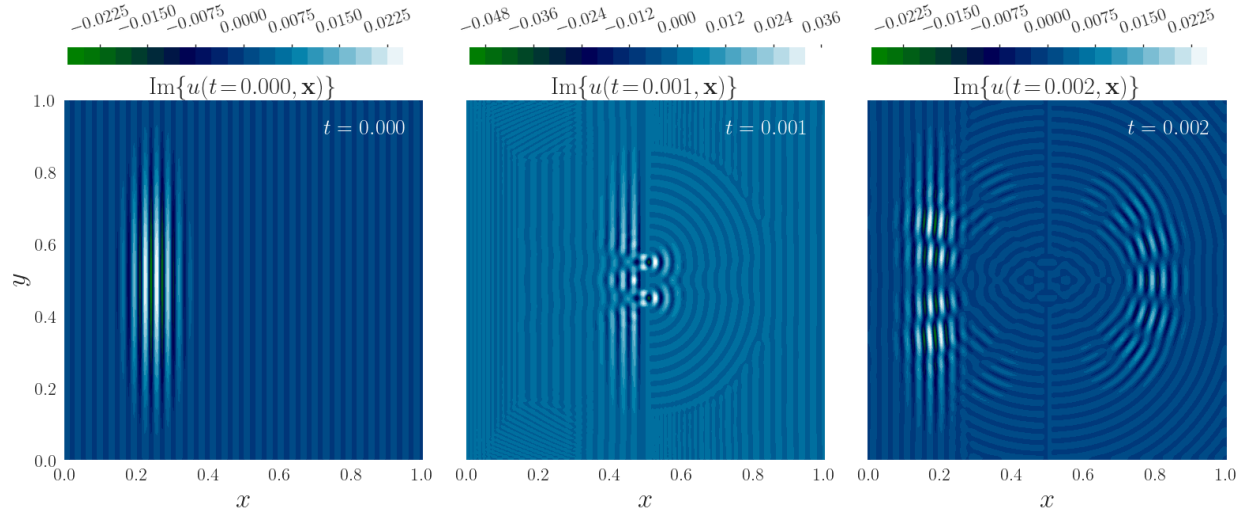

(c) *DS2*: Snapshots representing the evolution of the imaginary part of the wave function in position space.

FIG. 2: Colour maps showing the solution of the Schrödinger equation for the *DS2* setup at times $t = 0.000,\ 0.001,\ 0.002$. Pay attention to the varying colour bar scale from frame to frame.

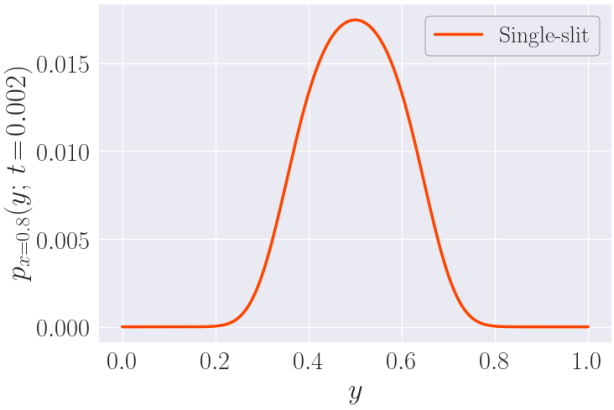

(a) *SS*: The probability along the y-axis for the single-slit experiment.

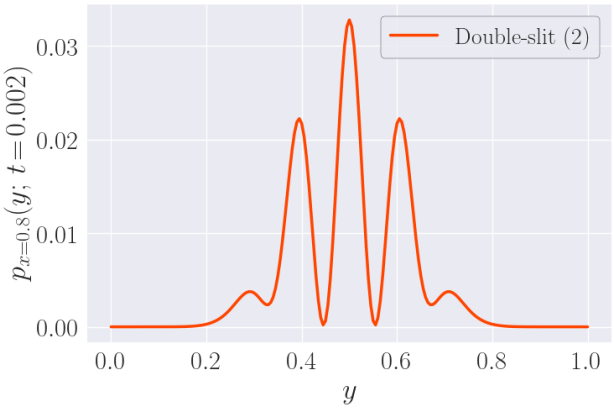

(b) *DS2*: The probability along the y-axis for the double-slit (2) experiment.

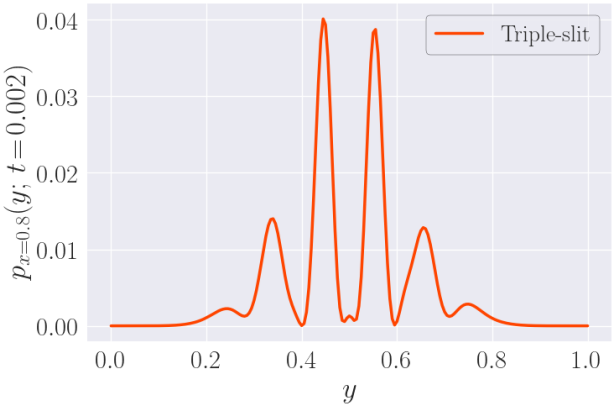

(c) *TS*: The probability along the y-axis for the triple-slit experiment.

FIG. 3: The amplitude for detecting the particle at vertical positions y at time $t = 0.002$ given that it is located at horisontal position $x = 0.8$, that is the quantity $p_{x=0.8}(y; 0.002)$ obeying equation (15), for simulations with one, two and three slits, but otherwise equal parameters.

scope of durations we consider, and does not seemingly tend to increase. This is an indication of a robust algorithm and a stable solution. The scattering pattern on the detector screen is consistent with results from well-known excrements. Future work might explore other sorts of wave packets. Our approach should be straightforwardly generalised to work in three dimensions, with the caveat of high computational expense. Experimenting with both the temporal and spatial solution could also be useful.

Appendix A: Discretisation

Suppose you want to solve the (1+1)-dimensional PDE

$$\frac{\partial u}{\partial t} = F\,; \quad F = F(t, x, u, \frac{\partial u}{\partial x}, \frac{\partial^2 u}{\partial x^2}), \tag{A1}$$

where $u = u(t, x)$. Let Δt be the time step size in the discretised verison of equation (A1). The Crank-Nicolson scheme can be viewed as a combination of the forward and backward Euler method, respectively at current and subsequent time step, and reads [2]:

$$\frac{u_i^{(n+1)} - u_i^{(n)}}{\Delta t} = \frac{1}{2}\left(F_i^{(n+1)} + F_i^{(n)}\right), \tag{A2}$$

where $u_i^{(n)} = u(n\Delta t, i\Delta x)$ and $F_i^{(n)}$ is F evaluated for i, n and $u_i^{(n)}$.

In our (2+1)-dimensional case where $u = u(t, \mathbf{x})$ we have

$$\frac{\partial u}{\partial t} = F(t, \mathbf{x}, u, \nabla^2 u) = \mathrm{i}\left(\nabla^2 u - v(\mathbf{x})u\right), \tag{A3}$$

and this approach translates to

$$\frac{u_{i,j}^{(n+1)} - u_{i,j}^{(n)}}{\Delta t} = \frac{1}{2}\left(F_{i,j}^{(n+1)} + F_{i,j}^{(n)}\right) \tag{A4}$$

where $u_{i,j}^{(n)} = u(n\Delta t, \mathbf{x}_{i,j})$, $\mathbf{x}_{i,j} = h(i, j)$, as in section III A 1, and $F_{i,j}^{(n)}$ is the right-hand side of equation (A3), explicitly:

$$F_{i,j}^{(n)} = \mathrm{i}\left(\left[\frac{\partial^2 u}{\partial x^2}\right]_{i,j}^{(n)} + \left[\frac{\partial^2 u}{\partial y^2}\right]_{i,j}^{(n)} - v_{i,j}u_{i,j}^{(n)}\right); \tag{A5}$$

Let h be the minimal separation between to points on the lattice. We approximate the two spatial second derivatives at a time step n as follows:

$$\left[\frac{\partial^2 u}{\partial x^2}\right]_{i,j}^{(n)} \approx \frac{1}{h^2}\left(u_{i+1,j} - 2u_{i,j} + u_{i-1,j}\right)^{(n)}; \tag{A6a}$$

$$\left[\frac{\partial^2 u}{\partial y^2}\right]_{i,j}^{(n)} \approx \frac{1}{h^2}\left(u_{i,j+1} - 2u_{i,j} + u_{i,j-1}\right)^{(n)}; \tag{A6b}$$

Define $r \equiv \frac{\mathrm{i}\Delta t}{2h^2}$. Further, let

$$\begin{aligned}\mathcal{F}_{i,j}^{(n)} = \;& r\left(u_{i+1,j} - 2u_{i,j} + u_{i-1,j}\right)^{(n)} \\ & + r\left(u_{i,j+1} - 2u_{i,j} + u_{i,j-1}\right)^{(n)} \\ & - \frac{\mathrm{i}\Delta t}{2} v_{i,j}\, u_{i,j}^{(n)}.\end{aligned} \tag{A7}$$

Equation (A4) becomes:

$$u_{i,j}^{(n+1)} - \mathcal{F}_{i,j}^{(n+1)} = u_{i,j}^{(n)} + \mathcal{F}_{i,j}^{(n)}; \tag{A8}$$

This final discretisation is valid for any step in time within the time range ($n \in [0, N_t - 2]$) and all internal points on the grid ($i, j \in [1, M - 2]$).

Appendix B: A and B matrices

In order to generalise the Crank-Nicolson approximation to the Schrödinger equation as a matrix equation $A\mathbf{u}^{(n+1)} = B\mathbf{u}^{(n)}$, that satisfy the Dirichlet boundary conditions on a discretised grid, we require A and B to take specific forms. We need both of them to be square matrices with dimensions $((M-2)^2 \times (M-2)^2)$, with vectors $\mathbf{a}$ and $\mathbf{b}$ as diagonals. These are given by:

$$\begin{aligned} a_k &= 1 + 4r + \frac{\mathrm{i}\Delta t}{2} v_{i,j} \\ b_k &= 1 - 4r - \frac{\mathrm{i}\Delta t}{2} v_{i,j}, \end{aligned} \tag{B1}$$

where r is still $r \equiv \frac{\mathrm{i}\Delta t}{2h^2}$. We fill the matrices A and B with $\pm r$-values along the first and third super- and subdiagonal; A with $-r$ and B with $+r$. Every $(M-2)$-th element along the first super- and subdiagonal for each matrix must be zero. For demonstrative purposes, if $(M-2) = 3$, A and B would look like the following:

$$A = \begin{bmatrix} a_0 & -r & 0 & -r & 0 & 0 & 0 & 0 & 0 \\ -r & a_1 & -r & 0 & -r & 0 & 0 & 0 & 0 \\ 0 & -r & a_2 & 0 & 0 & -r & 0 & 0 & 0 \\ -r & 0 & 0 & a_3 & -r & 0 & -r & 0 & 0 \\ 0 & -r & 0 & -r & a_4 & -r & 0 & -r & 0 \\ 0 & 0 & -r & 0 & -r & a_5 & 0 & 0 & -r \\ 0 & 0 & 0 & -r & 0 & 0 & a_6 & -r & 0 \\ 0 & 0 & 0 & 0 & -r & 0 & -r & a_7 & -r \\ 0 & 0 & 0 & 0 & 0 & -r & 0 & -r & a_8 \end{bmatrix} \tag{B2}$$

$$B = \begin{bmatrix} b_0 & r & 0 & r & 0 & 0 & 0 & 0 & 0 \\ r & b_1 & r & 0 & r & 0 & 0 & 0 & 0 \\ 0 & r & b_2 & 0 & 0 & r & 0 & 0 & 0 \\ r & 0 & 0 & b_3 & r & 0 & r & 0 & 0 \\ 0 & r & 0 & r & b_4 & r & 0 & r & 0 \\ 0 & 0 & r & 0 & r & b_5 & 0 & 0 & r \\ 0 & 0 & 0 & r & 0 & 0 & b_6 & r & 0 \\ 0 & 0 & 0 & 0 & r & 0 & r & b_7 & r \\ 0 & 0 & 0 & 0 & 0 & r & 0 & r & b_8 \end{bmatrix} \tag{B3}$$

By construction (and inspection), we notice that A and B are the complex conjugates of each other, and that A is a diagonally dominant matrix: $|a_{i,i}| > \sum_{j \neq i} |a_{i,j}|$ for each row in A.

[1] Berryman, S. (2016). Democritus.

[2] Crank, J., Nicolson, P., and Hartree, D. R. (1947). A practical method for numerical evaluation of solutions of partial differential equations of the heat-conduction type. Proceedings of the Cambridge Philosophical Society, 43(1):50.

[3] Hjort-Jensen, M. (2015). Computation physics, lecture notes fall 2015.

[4] Li, X. S. (2005). An overview of SuperLU: Algorithms, implementation, and user interface. ACM Transactions on Mathematical Software, 31(3):302–325.

[5] O'Connor, J. (2022). Quantum mechanics history.